

# SOME NEW CONCEPTS OF THE RELATION BETWEEN FIBRE ORIENTATION, FIBRE GEOMETRY, AND MECHANICAL PROPERTIES

R.W. Perkins and R.E. Mark  
Syracuse University, New York, USA

Following the initial work of Cox<sup>(1)</sup>, a number of studies has been carried out with the objective of predicting the in-plane mechanical behaviour of paper in terms of the geometrical structure of the fibre network and the mechanical properties of the fibres. Recently Perkins<sup>(2)</sup> developed a self-consistent model based on the straight segments of the fibres. As shown in figure 1, a typical fibre consists of several straight segments of lengths,  $l_{s1}, l_{s2}, \dots$

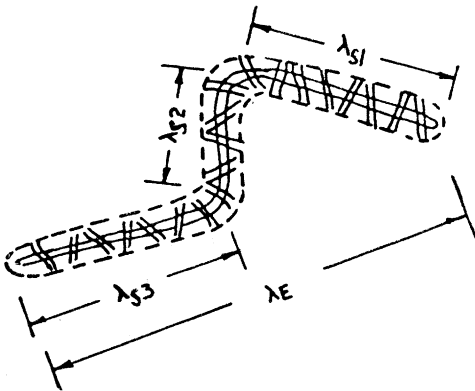


Fig 1—Schematic of fibre having 3 distinct segments; numerous crossing fibres are in contact with it.

The sum of the segment lengths equals the total fibre length  $l_T$ . The in-plane fibre curl,  $C$ , is defined in terms of the end-to-end length  $l_E$  and  $l_T$  viz

$$C = \frac{l_T - l_E}{l_T} \quad (1)$$

It is assumed that the fibres are sufficiently flexible in bending that no appreciable load can be transmitted from one straight segment to the next. Therefore, from a mechanics viewpoint, at least for small strains,

the straight segments behave as independent elements.

In the event that a fibre has micro-compressions or other damaged regions along its length, the locations of these regions also determine the ends of the load bearing segments even though the fibre is perfectly straight. The segment elements are coupled to the network by means of the crossing fibres. The strains of the sheet are presumed to be transmitted to the segment elements by means of bending and shearing deformation of the crossing fibres and shearing deformation of the fibre-to-fibre bonds. Thus, the axial strain in the segment elements is not uniform but varies from the segment ends where it is zero to the middle where it has its maximum value. If the segment is long enough and if the coupling of the crossing fibres is strong, the axial strain in the middle of a segment will be the same as the normal component of strain of the sheet for the direction of the segment. On the other hand, if the segment is short and/or the coupling is weak, the segment strain will be less than that associated with the sheet.

The model is further illustrated by figure 2, which shows a portion of a segment that is coupled by two crossing fibres to the remainder of the network. The boundary between the element and the network is depicted by a dashed line located a distance  $e$  from the centre-line of the segment. The symbol  $e$  represents the centre-to-centre distance between bonds along a typical fibre. If  $e$  is small in comparison with the fibre width  $w_f$ , as would be expected in moderately dense paper, the coupling is primarily attributable to the shearing deformations of the fibre-to-fibre bonds. In a very low density system such as tissue paper, the bending and shearing deformation of the crossing fibres may be substantial.

It is shown by Perkins<sup>(2)</sup> that the fibre stress  $\sigma_f$  and fibre strain  $e_f$  can be expressed as

$$\sigma_f = E_f^a e_f \quad (2)$$

$$e_f = e_s \left[ 1 - \frac{\cosh(a\zeta)}{\cosh(aL)} \right] \quad (3)$$

where  $E_f^a$  is the effective fibre axial modulus,  $\xi$  represents the distance from the segment centre,  $L$  is the half-segment length, and  $a$  is a coupling coefficient.

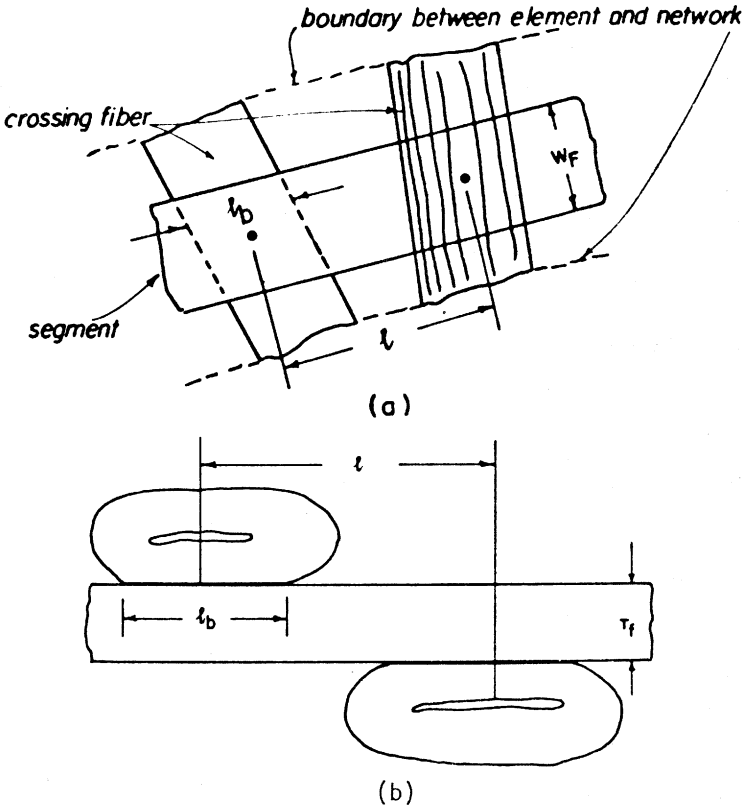


Fig 2—Portion of an element of a fibre segment illustrating the bond length along a fibre  $l_b$ , the centre-to-centre distance between bonds along a fibre  $l$ , the (dashed line) boundary between the segment element and the remainder of the network, the fibre width  $w_f$ , and the thickness  $r_f$ .

The strain

$$e_s = e_x \cos^2\theta + e_y \sin^2\theta + 2e_{xy} \sin\theta \cos\theta \quad (4)$$

represents the sheet strain in the direction corresponding to the orientation of the segment relative to the machine direction (see figure 3) and the sheet strains  $e_x$ ,  $e_y$ ,  $e_{xy}$ .

Y (cross-machine direction)

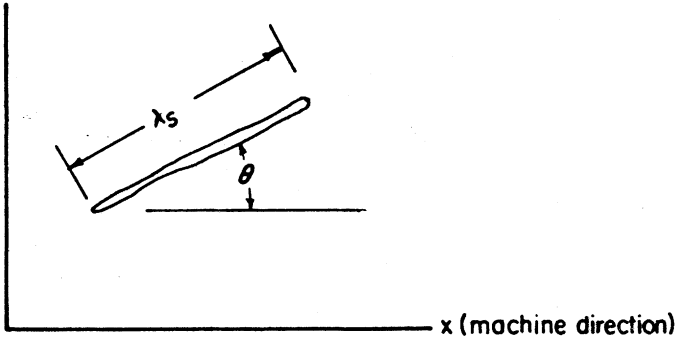


Fig 3—A segment of length  $\lambda_s$  and orientation  $\theta$ .

The effective axial fibre modulus  $E_f^a$  is given by

$$E_f^a = \frac{(e/e_b) (E_{fL} + E_{fT})}{1 + \frac{\tanh B}{B} + \left( \frac{E_{fL} + E_{fT}}{E_{fL}} \right) \left( \frac{e - e_b}{e_b} \right)} \quad (5)$$

$$B = \frac{1}{2} \sqrt{\left( \frac{e_b^2}{t_f t_b} \right) \left( \frac{G_B}{E_{fT}} \right) \left( 1 + \frac{E_{fT}}{E_{fL}} \right)} \quad (6)$$

where  $E_{fL}$ ,  $E_{fT}$ ,  $G_B$  represent the elastic moduli in the axial and transverse directions of the fibre and the shear modulus of the bond material, respectively. The dimension  $t_b$  represents the effective thickness of the fibre-to-fibre bond. The effective fibre modulus  $E_f^a$  depends on the axial elastic modulus of the cell wall material and also on the transverse cell wall elastic

modulus. The latter influence is the result of a reinforcing effect of the crossing fibres that are coupled to the segment through the fibre-to-fibre bond.

The quantity  $a$  in equation (3) describes the axial force coupling between the network and the segment by virtue of the crossing fibres and fibre-to-fibre bonds. It is convenient to write

$$a = \frac{k_f}{A_f E_f} \quad (7)$$

where  $A_f$  is the fibre cross-sectional area and

$$k_f = \frac{2}{\left( e \frac{(e - e_b)^3}{12E_{fL} I_f} \left( 1 + \frac{12E_{fL} I_f}{G_f A_f e^2} \right) + \frac{2t_b}{A_b G_b} \right)} \quad (8)$$

Here  $I_f$  represents the moment of inertia associated with the fibre cross section,  $G_f$  represents the cell wall shear modulus,  $f$  is a factor that depends upon the fibre cross-sectional shape (it is 6/5 if the fibre has a rectangular shape), and  $A_b$  is the area of the fibre-to-fibre bond.

In accordance with the self-consistent scheme, the strain energy of a typical segment element is calculated as

$$W_e = 0.5 E_f^a A_f l_s e_s^2 \eta_L \quad (9)$$

where

$$\eta_L = 1 - \frac{1}{2} \frac{\tanh(aL)}{aL} - \frac{1}{2 \cosh^2(aL)} \quad (10)$$

can be identified as a coupling efficiency. For strong coupling and long length,  $\eta_L$  approaches unity. At the other extreme of very short length or very weak coupling, it approaches zero.

The total strain energy of the system can be written

$$W = \int_0^{\infty} \int_0^{\pi} D_0 f_{\theta l_s}^* W_e d\theta dl_s \quad (11)$$

where  $D_0$  represents the number of segment elements per unit area and  $f_{\theta l_s}^* d\theta dl_s$  represents the probability of finding a segment having a length in the interval  $l_s, l_s + dl_s$  and orientation in the interval  $\theta, \theta + d\theta$ . In general, it is expected that the length and orientation effects are coupled (cf. Carroll<sup>(3)</sup>).

Suppose that  $f_{\theta l_s}^*$  can be expressed in the form

$$f_{\theta l_s}^* = (f_{\theta}(a_1, a_2, \dots, a_m))(f_{l_s}(l_s, b_1, b_2, \dots, b_n)) \quad (12)$$

Thus,  $f_{\theta}$  describes the fibre orientation distribution as a function of  $\theta$  depending on the  $n$  parameters  $a_1, a_2, \dots, a_m$ . Likewise, the distribution of fibre lengths  $l_s$  depends on  $n$  parameters  $b_1, b_2, \dots, b_n$ . In general, it is to be suspected that the parameters  $a_1, a_2, \dots, a_m$  are functions of  $l_s$  while the parameters  $b_1, b_2, \dots, b_n$  are functions of  $\theta$ . The evidence presently available suggests that the coupling between the two distributions is weak and therefore, as an approximation valid at least for certain papers, it is acceptable to assume that the length and orientation distributions are independent. For this assumption, the parameters  $a_1, a_2, \dots, a_m$  and  $b_1, b_2, \dots, b_n$  are constants, and the strain energy per unit sheet area can be written in the form

$$W = \frac{1}{2} \frac{\omega_s}{\rho_f^a} \int_0^{\pi} \varphi_{l_s} E_f^a e_{f_s}^2 f_{\theta} d\theta \quad (13)$$

where  $\omega_s$  represents the basis weight,  $\rho_f^a$  represents the apparent fibre density and

$$\varphi_{l_s} = \int_0^{\eta_L} f_{l_s} dl_s \quad (14)$$

The length parameter  $\varphi_{1s}$  and the apparent fibre modulus  $E_f^a$  may depend upon the orientation direction  $\theta$  as a result of the stresses that may be imposed on the fibres during the drying of the sheet during manufacture. In order to take this phenomenon into account analytically, we can assume that the apparent fibre modulus  $E_f^a$  depends upon the shrinkage and restraint conditions present during drying in the following way:

$$E_f^a = E_{f0}^a (1 + H e_{ND}) \quad (15)$$

where  $E_{f0}^a$ , a constant, represents the apparent fibre modulus in the absence of drying restraint,  $H$  is a constant that predicts the magnitude of stiffening due to drying restraint and

$$e_{ND} = (a_x M + e_{xD}) \cos^2 \theta + (a_y M + e_{yD}) \sin^2 \theta \quad (16)$$

Here  $a_x M$  and  $a_y M$  represent the sheet shrinkage strains during unrestrained drying in the  $x$  and  $y$  directions,  $e_{xD}$  and  $e_{yD}$  represent the sheet strain that is applied or allowed during shrinkage. Thus, for unrestrained shrinkage conditions

$$e_{xD} = -a_x M \text{ and } e_{yD} = -a_y M$$

It is evident that  $e_{ND}$  is related to the magnitude of restraint that a fibre of orientation  $\theta$  would be subjected to during the drying of the sheet. In the following, it is further assumed that  $e_{ND}$  is positive, i.e., that the fibres are loaded in tension as a result of any drying restraint.

With the help of relation (15), the integration in (13) can be easily carried out, provided the length factor  $\varphi_{1s}$  is independent of  $\theta$ . In fact  $\varphi_{1s}$  does depend on  $\theta$  because the coupling parameter  $a$  that appears in  $\eta_L$  depends on  $E_f^a$ . Fortunately, however, the influence of variation in  $E_f^a$  through  $a$  in  $\varphi_{1s}$  has an insignificant effect on the predictions of the elastic moduli of the sheet and there is no serious error committed in assuming that  $\varphi_{1s}$  is independent of  $\theta$ .

The stress-strain relations for the sheet can be obtained from the strain energy function  $W$  after carrying out the integration through the relations

$$T_x = \frac{\partial W}{\partial e_x}, \quad T_y = \frac{\partial W}{\partial e_y}, \quad T_{xy} = -\frac{1}{2} \frac{\partial W}{\partial e_{xy}} \quad (17)$$

where  $T_x$ ,  $T_y$ , and  $T_{xy}$  represent the force per unit edge length of the paper sheet. In order to express conveniently the resulting elastic moduli it is desirable to express the orientation distribution  $f_\theta(\theta)$  in terms of the expansion of its Fourier series (Cox<sup>(1)</sup>). When the  $x$ -direction is one of the axes of elastic symmetry, e.g. the machine direction, and  $\theta = 0^\circ$  corresponds to this direction,

$$f_\theta(\theta) = \frac{1}{\pi} (1 + a_1 \cos 2\theta + a_2 \cos 4\theta + \dots + a_n \cos 2n\theta + \dots) \quad (18)$$

After using (18) and (15) in (13) and subsequently using (17), the Young's moduli  $E_x^*$ ,  $E_y^*$ , the shear modulus,  $G_{xy}^*$ , and the Poisson ratios  $\nu_{xy}$ ,  $\nu_{yx}$  corresponding to plane stress loading of the sheet are found to be:

$$E_x^* = \frac{1}{16\rho} \frac{\omega_s}{f} \frac{a}{1s} E_{f0} \left[ (1 + \langle e \rangle) (6 + 4a_1 + a_2) + \frac{e}{2} (8 + 7a_1 + 4a_2 + a_3) \right] \begin{bmatrix} 1 - \nu_{xy} & \nu_{yx} \\ \nu_{xy} & 1 \end{bmatrix}$$

$$E_y^* = \frac{1}{16\rho} \frac{\omega_s}{f} \frac{a}{1s} E_{f0} \left[ (1 + \langle e \rangle) (6 - 4a_1 + a_2) - \frac{e}{2} (8 - 7a_1 + 4a_2 - a_3) \right] \begin{bmatrix} 1 - \nu_{xy} & \nu_{yx} \\ \nu_{xy} & 1 \end{bmatrix}$$

$$\nu_{xy} = \frac{(1 + \langle e \rangle) (2 - a_1) + \frac{e}{4} (a_1 - a_3)}{(1 + \langle e \rangle) (6 - 4a_1 + a_2) - \frac{e}{2} (8 - 7a_1 + 4a_2 - a_3)}$$

$$\nu_{yx} = \frac{(1 + \langle e \rangle) (2 - a_1) + \frac{e}{4} (a_1 - a_3)}{(1 + \langle e \rangle) (6 + 4a_1 + a_2) + \frac{e}{2} (8 + 7a_1 + 4a_2 + a_3)}$$

$$G_{xy}^* = \frac{1}{16\rho} \frac{\omega_s}{f} \frac{a}{1s} E_{f0} \left[ (1 + \langle e \rangle) (2 - a_1) + \frac{e}{2} (a_1 - a_3) \right]$$

where

$$\begin{aligned} \langle e \rangle &= \frac{1}{2} H \left[ (a_x^M + e_{xD}) + (a_y^M + e_{yD}) \right] \\ e &= \frac{1}{2} H \left[ (a_x^M + e_{xD}) - (a_y^M + e_{yD}) \right] \end{aligned} \quad (20)$$

It will be noted from an inspection of relations (19) that the elastic constants depend only on the first three parameters  $a_1, a_2, a_3$  that occur in the Fourier series expansion for  $f_\theta$ . It will be noted further that if the influence of drying restraint is not incorporated or if the sheet is dried under conditions of no restraint, then the elastic moduli depend only on the parameters  $a_1$  and  $a_2$ . For this condition, relations (19) are essentially the same as those given by Cox<sup>(1)</sup> when  $\theta = 0^\circ$  corresponds to a direction of elastic symmetry in the sheet. The number of coefficients of the Fourier series expansion for  $f_\theta$  that are necessary for predicting the elastic properties, therefore, depends on the functional relation between the apparent fibre modulus  $E_f^a$  and orientation, which in turn depends on the procedures and conditions of drying. If any other phenomena are incorporated that influence the angular dependence of the factors entering the calculation for the strain energy stored in the sheet, then the number of Fourier coefficients appearing in the elastic constants will also be changed.

It is theoretically possible to describe any fibre orientation distribution in terms of the parameters  $a_1, a_2, a_3, \dots$  of the Fourier series expansion. There is a real advantage, however, in using a function with only one parameter, since this choice will reduce the expressions for the elastic moduli to forms that depend on one parameter in so far as orientation anisotropy is concerned. The reduction to one parameter can be accomplished very simply by truncating the Fourier series and retaining the single parameter  $a_1$ . This procedure was employed by Corte and Kallmes<sup>(4)</sup> and by Perkins<sup>(2)</sup>. It will be noted, however, that the reduction to a single parameter can have some significant effects. For example, for the case of a freely dried paper, the shear modulus should

decrease with increased anisotropy. This reduction effect will be predicted only if the coefficient  $a_2$  is retained in the expansion, Eq.(18). But if only one parameter of the Fourier series expansion is used, the shear modulus is predicted to be independent of the degree of anisotropy of the paper.

An alternative approach is to employ a distribution function that has only one shape parameter. Forgacs and Strelis<sup>(5)</sup> employed a distribution with the behaviour of an ellipse, called the elliptical distribution. Mardai<sup>(6)</sup> describes a number of single parameter functions that can be used to describe angular data. Among these, the von Mises distribution seems to have the most promise for describing the fibre orientation distribution in paper. The properties and behaviour of the elliptical and von Mises distributions are treated in detail below.

It is evident from the foregoing that fibre orientation distribution is generally of great importance relative to the elastic (and other mechanical) properties of the paper sheet. Its influence has been studied extensively<sup>(1-5,7-14)</sup>. It also appears evident that the choice of distribution function used to represent fibre orientation has some serious implications relative to our ability to predict the elastic constants for sheets of different fibre alignment configurations. On the other hand, the distribution of lengths of the fibres may or may not be very significant in different cases. We now consider improvements in the acquisition and interpretation of experimental data for these length and orientation distributions.

#### **Methods for Fibre Orientation Determination**

The initial work done in this field was by Danielsen and Steenberg<sup>(15)</sup>, who developed a sort of rotatable protractor for directly measuring the orientations of dyed fibres that are added to the furnish when the sheet is made. The dyed fibres, amounting to less than 1%, are typical of the pulp stock used and are measured as a representative sample of the whole. Subsequently, other workers modified the Danielsen-Steenberg

method and introduced several indirect methods, including x-ray diffraction, light scattering, zero-span tensile, and optical diffraction analysis. In the methods of Forgacs and Strelis<sup>(5)</sup> and Corte and Kallmes<sup>(4)</sup>, counts are made of the numbers of dyed fibres falling on straight reference lines. These counts provide indirect data that are converted to orientation distribution functions via mathematical treatment of the data.

It became apparent to us that there are unresolved problems related to the indirect methods and that none of the manual methods would permit us to collect and analyse a meaningful number of data within a reasonable time frame. Also, serious questions arose concerning the accuracy of indirect methods such as the line crossing techniques employed by Corte and Kallmes<sup>(4)</sup>. Fortunately, measuring devices developed within the past few years have enabled us to accelerate and automate the collection of data. In our case, this is accomplished through the use of a graphic digitiser, which is basically a device for rapid and accurate reading of co-ordinates.

### First Principles

Determination of the orientation of fibres by any direct method required some preliminary decisions as to what types of information are needed, e.g.,

#### 1. What is to be measured?

Given that fibres in a sheet of paper or paper-board are of finite (short) length, and usually contain bent, curled, or broken sections, one has to make a decision as to what constitutes a 'fibre' for purposes of determining fibre orientation. The same statement can be made regarding determination of fibre length, and it should be emphasised that there is no basis a priori for assuming that fibre length and orientation are independent of each other. These parameters may, in fact, be highly correlated in some cases.

With reference to figures 4 and 5, one may observe several possibilities for defining the fibre in terms of orientation. Each possibility has different implications for length categorisation.

Figure 4 shows a sheet in which a small fraction (ca. 0.25%) of black dyed fibres show contrast against the remaining 99.75%, which are bleached. The paper samples are impregnated with silicone oil (with or without the assistance of vacuum) to enhance visibility of the dyed fibres by making the rest of the sheet almost transparent. (The refractive indices of the oil and the fibres are nearly equal.) The orientation of the fibre labeled "F", for example, may be described in any one of the following ways:

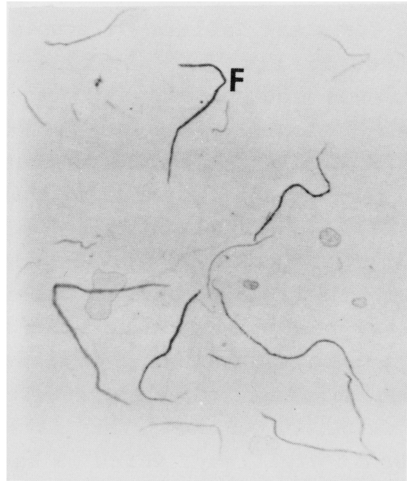


**Fig 4**—Photograph of oil-impregnated sheet. Black-dyed fibres at various depths in the sheet stand out. (Photo by A. Eusufzai)

With respect to a fixed axis (e.g., the machine direction) the orientation of a straight line joining the ends of the fibre, Fig. 5a.

With respect to a fixed axis, the orientation of the "best fit" of all the segments of a fibre together. Essentially a regression line is drawn that best fits a set of points taken to lie at the midpoint of each segment of the fibre, Fig. 5b.

With respect to a fixed axis, the orientation of each segment of the fibres taken individually, Fig. 5c.

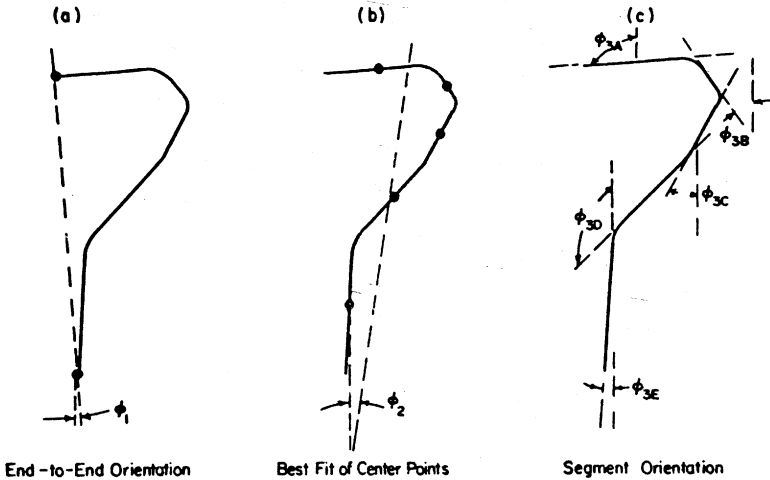


Fig 5—Diagrammatic representation of dyed fibre F in Figure 1. (a) Black circles = end points, dashed lines = end-to-end distance,  $\phi_1$  = orientation of fibre in sheet. (b) For computational purposes, fibre is divided into 5 segments. Black circles = segment mid-points, dashed line = regression line of midpoints,  $\phi_2$  = orientation of fibre in sheet by best fit of centrelines. (c) Orientation  $\phi_{3j}$  determined for each segment.

With respect to a fixed axis, the orientations of segments according to length category. In such cases, criteria have to be set as to how many segment length categories are needed. For example, a preliminary study can be made to determine the most probable (statistically) segment length encountered in a given type of sheet material. One can establish the length categories according to some system based on most probable length (mpl). For example:

Segment group 1:  $0 < l \leq l_{mpl}$   
 Segment group 2:  $l_{mpl} < l \leq 2l_{mpl}$   
 Segment group 3:  $2l_{mpl} < l \leq 3l_{mpl}$   
 Segment group 4:  $3l_{mpl} < l$

The four modes of description itemised above are listed in increasing order of precision results obtained, assuming an adequate sample size is taken. However, the difficulty of measurement also increases in the same order.

## 2. What sector size is needed?

The frequency with which fibres or fibre segments are found with alignments falling in a given range (radians or degrees) is usually the immediate objective of the experiment or proof. Pre-selection of an angular interval that enables a comprehensive, accurate picture of fibre orientation distribution is essential. A very commonly selected interval is 5 degrees.

## 3. How are representative samples to be obtained?

If possible, the incorporation of a small percentage (0.10 - 0.25%) of dyed fibres into the sheet is desirable. For many purposes, a chlorazol black E dye is excellent. These dyed fibres stand out among the other fibres, as shown in figure 4. The use of dyed fibres makes it possible to cross-check accurately against other methods of determination.

If it is not possible to incorporate any type of individually identifiable fibre into the sheets to be tested, one of the indirect methods will have to be used. However, it is important that when any indirect method is considered for use on a particular material, an independent verification is made that the indirect method will yield results in agreement with a direct method.

4. How will the data be compiled?

## (a) Angular distribution frequency

Usually fibre orientation data have to be compared or fitted to a generally bimodal (symmetrical with respect to the machine direction) mathematical function of some form to be useful. As noted earlier, distribution functions that have been used or suggested for use with fibre networks include the cosine<sup>(4)</sup> elliptical<sup>(5)</sup> and von Mises<sup>(6)</sup>.

The goodness with which any of these functions will fit a set of experimental data for fibre orientation depends on the degree of anisotropy of the sheet, the scatter in the experimental data, and the shape parameter(s) for the function. Some explanation of these functions and parameters will illustrate this point.

Elliptical

The elliptical distribution function has the form:

$$f(\theta) = \frac{\zeta}{\pi} (1 / (\cos^2\theta + \zeta^2 \sin^2\theta)) \quad (21)$$

The degree of ellipticity of this function is controlled by the shape parameter,  $\zeta$ , which is equal to the ratio of the major and minor semi-axes. Selection or determination of an appropriate value for  $\zeta$  enables one to fit a curve to the probability density of finding a fibre within a given (say 5 degree) sector of orientation. The determination of  $\zeta$  is usually accomplished by use of a least square error method when the elliptical function is fitted to the observed data. Allowable values of  $\zeta$  are never less than unity. The symbol  $\theta$  refers to the angle of orientation. It varies from  $-90^\circ$  to  $+90^\circ$  when the machine direction is taken to be  $0^\circ$ . Plotted in Cartesian form, the elliptical function will generate a smooth, rounded-peak curve. When plotted in polar coordinates, the function generates an ellipse, of course.

.. Cosine

As noted previously, there is a useful distribution function consisting of a series expansion of cosine terms of the form:

$$f(\theta) = \frac{1}{\pi} (1 + a_1 \cos 2\theta + a_2 \cos 4\theta + \dots + a_n \cos 2n\theta) \quad (22)$$

In this expression there is a series of shape parameters  $a_k$  that modify the basic curve form. With appropriate values for  $a_k$ , the function may be fitted to the experimental probability distributions (i.e., data points) sector by sector. In the work of Corte and Kallmes<sup>(4)</sup>, the series expansion was truncated to:

$$f(\theta) = \frac{1}{\pi} (1 + a_1 \cos 2\theta), \quad 0 \leq a_1 \leq 1 \quad (23)$$

for ease of mathematical manipulation. The form of eq. (23) is designated as 'single cosine term' in this paper. Plotted in polar co-ordinates, the form is bimodal cardioid. As will be observed, we have used this form and, additionally, a 'two cosine term' form, i.e.,

$$f(\theta) = \frac{1}{\pi} (1 + a_1 \cos 2\theta + a_2 \cos 4\theta) \quad (24)$$

for purposes of analysing our experimental data. In polar co-ordinates, the curve is cusped differently from the single cosine term. In Cartesian co-ordinates, eqs. (23) and (24) generate symmetrical curves with rounded peaks. The determination of the shape parameters  $a_k$  in eqs. (22) to (24) can also be made using the least square error method. In eqs. (22) and (24), these shape parameters are subject to limits in allowable values that ensure that no negative probabilities are generated. In eq. (23), the limits are:

$$0 \leq a_1 \leq 1$$

... Von Mises

Another powerful function suited to the handling of the fibre orientation distribution data is known as the von Mises distribution; more specifically, the function used here is a multimodal distribution of the von Mises type (see ref.<sup>(6)</sup>). Here, the probability density function is given by:

$$f(\theta) = \frac{1}{\pi I_0(K)} e^{K \cos^2(\theta - \mu_0)} \quad (25)$$

where  $I_0(K)$  is a modified Bessel function of the first kind and order zero, i.e.

$$I_0(K) = \sum_{n=0}^{\infty} \frac{1}{(n!)} \left(\frac{K}{2}\right)^{2n} \quad (26)$$

Two parameters are present in eq.(25). The parameter  $\mu_0$ , which for our purposes may fall in the range  $-90^\circ$  to  $+90^\circ$ , establishes the mean direction, while  $K$  is a shape (density) parameter. The determination of parameters  $K$  and  $\mu_0$  is discussed by Mardia<sup>(6)</sup>. Allowable values of  $K$  must always be non-negative.

Since an increase in the anisotropy of the test material will result in a set of experimental points with a relatively high, narrow peak, while a more random sheet will show less variation between the MD and the other directions, it can be inferred that the value of the density parameter  $K$  will be larger for the distribution curve that approximates the points generated from the more orientated material. As for the other parameter,  $\mu_0$ , it can often be assumed that the greatest probability of finding a fibre orientated in a sector will correspond to the sector around the machine direction, for example, the interval  $-2.5^\circ$  to  $+2.5^\circ$ . If this is a valid assumption, then  $\mu_0 = 0$ . If the fibres are more orientated in the cross machine direction, then data plotted in the same way will approximate to a curve whose peak lies at  $90^\circ$  and  $\mu_0 = 90^\circ$ . In such cases,  $0$  will be taken for the interval  $0^\circ$  to  $180^\circ$ . For sheets formed under conditions wherein the greatest fibre alignment is neither MD nor CD,  $\mu_0$

will have to be determined according to the method described by Mardia<sup>(6)</sup>.

It should not be too readily assumed that  $\mu_0 = 0^\circ$  or  $90^\circ$ . Some paper machines, in fact, operate in a manner such that the greatest fibre alignment is not coincident with either MD or CD<sup>(8)</sup>. One of the advantages in fitting eq. (25) (for the von Mises distribution) to the experimental data is that the determination of  $\mu_0$  can serve as an indication if the sample edges are, in fact, aligned with the MD and CD directions in the cases where that is the intention. The elliptical and cosine functions can be similarly modified by replacing  $\theta$  with  $(\theta - \mu_0)$  in eqs. (21) to (24). The determination of  $\mu_0$  can at times provide insights that make it possible to correct faulty experimental or analytical procedures.

Once the true axes of orientation have been determined, the appropriate distribution function(s) (elliptical, cosine or von Mises) can be used as analytical tools to develop structure-property relationships with respect to the natural directions of symmetry. One important example is the precise determination and prediction of anisotropic elastic constants. Given the true orientation axes, the term  $\mu_0$  is set equal to zero from that point on. Accordingly, the Fourier expansion forms for the above mentioned distributions are very helpful. A Fourier expansion for the von Mises distribution has been given by Mardia<sup>(6)</sup>:

$$f(\theta) = \frac{1}{\pi I_0(K)} e^{K \cos 2\theta} = \frac{1}{\pi} \left[ 1 + 2 \sum_{n=1}^{\infty} \frac{I_n(K)}{I_0(K)} \cos 2n\theta \right] \quad (27)$$

where  $I_n(K)$  is a modified Bessel function of the first kind and order  $n$ . For the elliptical distribution, the Fourier series can be written as

$$f(\theta) = \frac{\zeta}{\pi} \left( \frac{1}{\cos^2 \theta + \zeta^2 \cos^2 \theta} \right) = \frac{1}{2} \left[ 1 + 2 \sum_{n=1}^{\infty} \left( \frac{\zeta - 1}{\zeta + 1} \right)^n \cos 2n\theta \right] \quad (28)$$

A comparison of eqs. (22), (27) and (28) shows that the  $n$ -term cosine function has  $n$  degrees of freedom, whereas the von Mises and elliptical functions each have a single degree only.

A polar diagram of the von Mises type distribution (eq. (27)) shows that it is bimodal when plotted in that manner. It is highly useful for curve-fitting a symmetrical plot of probability density versus orientation angle, as evidenced by the experimental results that follow.

For other possible distribution functions, refer to Mardia<sup>(6)</sup>.

(b) Length distribution

As each fibre is examined, data are accumulated that enable computation of the lengths of the fibre elements, since the end point co-ordinates are being digitised. Inherently it is possible to calculate fibre end-to-end length, fibre segment length, and total length based on summing of segment lengths. Fibre curl (cf. eq. (1)) can also be calculated from the accumulated data.

Typically, the type of length distribution data that are generated is in the form of a skewed curve when lengths are plotted versus frequency of occurrence. Such a curve can, in most cases, be readily fitted to an Erlang distribution function<sup>(15)</sup> using the least squares method.

The Erlang probability density function is

$$f(x) = \frac{(x/b)^{c-1} \exp(-x/b)}{b((c-1)!)}$$

where  $b$  = scale parameter, always greater than zero

$c$  = shape parameter, an integer greater than zero

$bc$  = mean value of  $x$ .

The range of the function is determined by

$$0 \leq x \leq +\infty$$

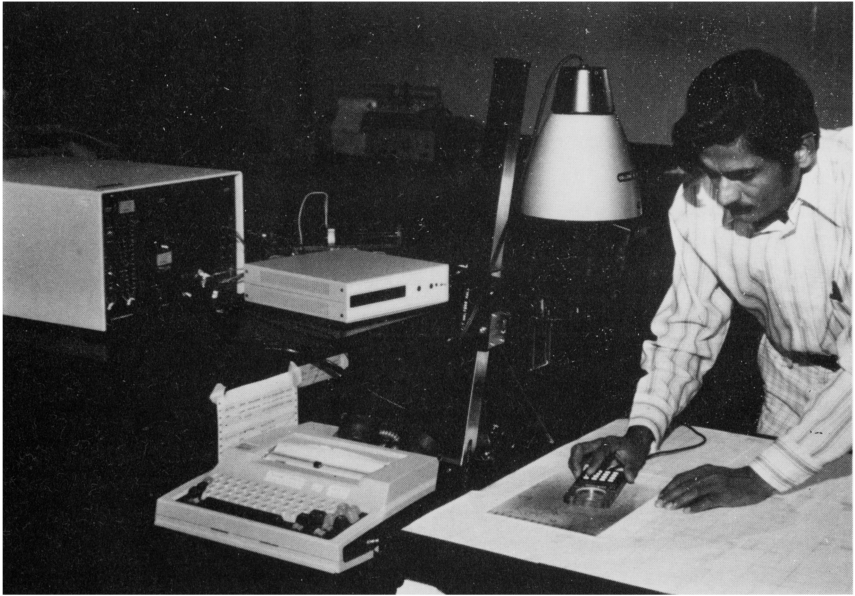
Graphic digitising system

Fig 6—Operation of graphic digitiser.

As mentioned earlier, the experimental data for fibre length and orientation is acquired by use of a graphic digitiser. The digitiser at ESPRI (figure 6), which is interfaced to the Syracuse University computer via a device coupler and remote terminal (figure 7), consists of a tablet, cursor with cross hair and control unit. An electronic grid in the tablet resolves any position on its unique x-y co-ordinates that can be identified by the use of the movable cursor. Resolution is 0.01 inch. Upon pressing one of the buttons on the cursor, two five-digit co-ordinates are output, along with a single hexadecimal 'signal' digit. The latter identifies which of the 16 buttons on the cursor was pressed, giving a method of classifying data pairs into categories for later processing.

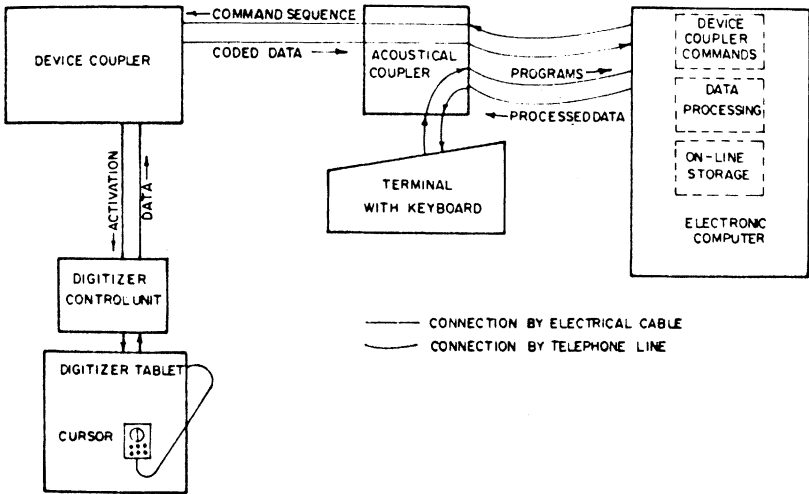


Fig 7—Schematic of graphic digitising system, including device coupler, terminal and computer.

If an enlarged print or other image of a sample sheet containing dyed fibres is displayed or projected on the tablet, certain points of interest can be identified by determining their co-ordinates. More importantly, the relationships among these co-ordinates can be established. For example, distances between fibre end points can be translated into lengths. For greater accuracy, several points along a fibre (logically those where the azimuth changes) can describe its length more accurately. Also angles between segments can be identified, as can angles between fibres and a predefined reference line (such as the machine direction). As multiple measurements are made, totals, means, and distributions become the parameters of interest.

Many digitiser installations include dedicated mini-computers built into the system. In our case it was decided to use the more extensive facilities available on a time-sharing basis,

specifically those of the Syracuse University computer centre. Access is gained through a typewriter-size terminal which accepts a standard telephone receiver. The connection with the computer is then made through telephone lines.

### **Applications of the Digitising Method in Experiments**

A series of experimental cylindrical sheets was prepared at the Swedish Forest Products Research Laboratory (STFI) using a 'Formette Dynamique' device. Samples measuring 279 mm x 216 mm were cut from these.

#### Sample specifications

Pulp: Bleached softwood kraft.

Basis weights: 10, 30, and 80 g/m<sup>2</sup>.

Anisotropy: Series 1-5 were prepared for each basis weight, the designation 1 being given to the least orientated and 5 to the most highly orientated specimens. The degree of orientation was controlled by varying the ratio of jet speed to wire speed.

Percentage of dyed fibres:  $\sim$  0.25

#### Procedure

From each sample, sub-samples 32 mm x 19 mm were removed, impregnated with silicone oil, and inserted in the film holder of a standard 35-mm photographic enlarger. The illuminating lamp of the enlarger projected the image of the dyed fibres directly onto the digitiser tablet (see figure 6). However, it should be emphasised that, although a film holder is used, no film is involved. What is projected onto the digitiser tablet is the image of all the dyed fibres in the sheet itself, since the oil impregnant renders them visible regardless of the depth at which they are located within the sheet. A flowchart of the subsequent digitising and computing operations is given in figure 8.

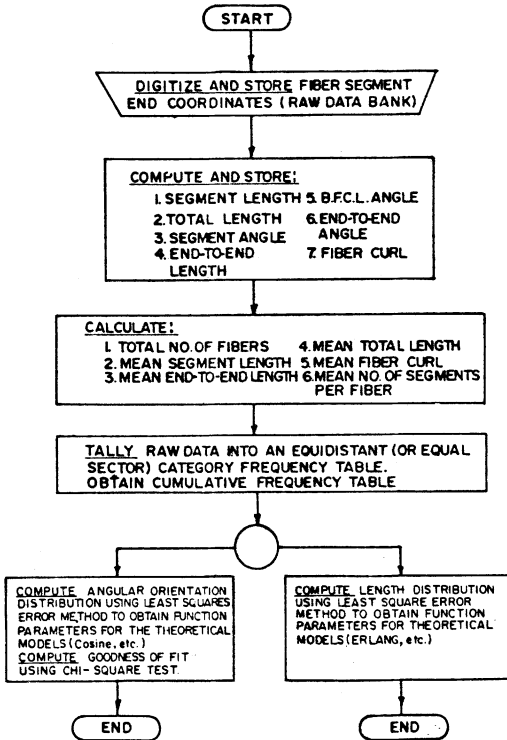


Fig 8—Flowchart for acquisition and processing of fibre orientation and length data.

We have found that for most of our calculations a sample size of 600 fibres is generally sufficient to yield results that are consistent and reproducible between different operators; however, a larger sample may be desirable when segment lengths and angles are measured. Earlier direct methods required the measurement of 2000 - 2500 fibres<sup>(8,15)</sup>.

### Results

The full series of sheets produced at STFI has been studied for mechanical properties, fibre orientation, and length distribution. In this paper we provide some illustrative values obtained for fibre orientation and length distributions: a complete set of values will appear in a forthcoming thesis<sup>(17)</sup>.

In Table 1 we present the statistics of the STFI specimen material as to: total number of fibres examined, mean number of segments per fibre, mean segment length, mean total length, mean end-to-end length, and mean fibre curl factor. These fibres show that about 600 fibres were observed for each type of specimen and that the average fibre has between 2 and 3 segments with

KEY: N = Total number of fibres examined  
 NS = Mean number of segments per fibre  
 LS = Mean segment length (mm)  
 LT = Mean total length (mm)  
 LE = Mean end-to-end length (mm)  
 FC = Mean fibre curl factor ( $FC = 1 - \frac{LE}{LT}$ )

	1-10	1-30	1-80	2-10	2-30	2-80
N	702	565	595	657	597	515
NS	2.22	2.02	2.23	2.03	2.40	2.37
LS	0.788	0.772	0.830	0.872	0.725	0.726
LT	1.75	1.56	1.85	1.77	1.74	1.72
LE	1.64	1.48	1.75	1.67	1.62	1.58
FC	0.063	0.051	0.054	0.056	0.069	0.081
	3-10	3-30	3-80	4-10	4-30	4-80
N	634	609	538	607	658	621
NS	2.30	2.15	2.46	2.28	2.32	2.24
LS	0.813	0.865	0.792	0.882	0.797	0.768
LT	1.87	1.86	1.95	2.01	1.85	1.72
LE	1.75	1.75	1.86	1.86	1.69	1.58
FC	0.064	0.059	0.046	0.074	0.086	0.081
	5-10	5-30	5-80			
N	612	703	611			
NS	2.50	2.28	2.28			
LS	0.684	0.811	0.732			
LT	1.71	1.85	1.67			
LE	1.61	1.77	1.58			
FC	0.058	0.043	0.054			

Table 1  
 Characteristics of dyed fibres in STFI sheets

distinctly different orientations. Fibre curl factors range from 0.043 to 0.086, indicating that the fibres in this particular pulp were not extensively curled.

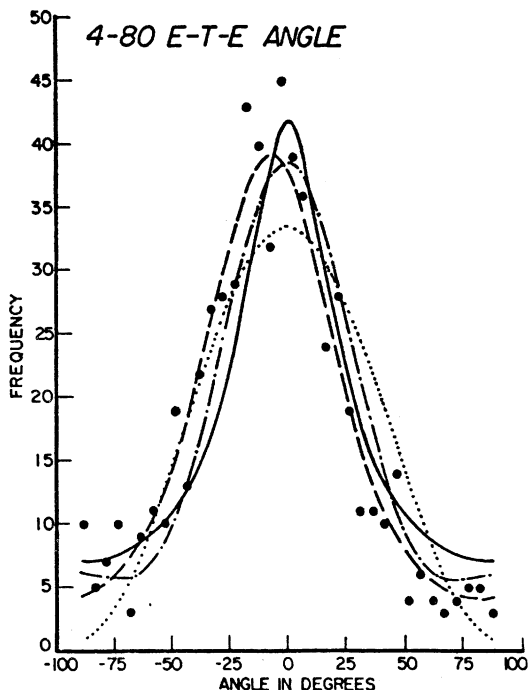


Fig 9—Frequency data for fibre end-to-end angular orientation measurements.

Legend: data (black circles), elliptical (solid), von Mises (dashed), two cosine (dot-dashed) single cosine (dotted)

As indicated previously, we have obtained experimental distribution data for angular orientation and length for all types of specimen material provided by STFI. Space does not permit us to tabulate all of the shape and scale factors, probabilities, and chi-square test results for all the orientations, basis weights, and curve-fitting techniques, nor present all the graphical data that go with these. Again, we refer to Chang's thesis<sup>(17)</sup>. We have instead, selected a particular type of material and present herewith some data and calculations pertaining to that type of specimen.

The specimen material selected was STFI-4-80.

Material designated by '4' has a moderately high degree of orientation (highest is 5): the 80 refers to the basis weight, 80 g/m<sup>2</sup>. The curves for 4-80 demonstrate typical effects observed in curve-fitting by various theoretical models, and some of the peculiarities of the various distribution functions are brought out in this set of curves. We feel that use of an 80 g/m<sup>2</sup> specimen demonstrates that good data can be generated even

with a moderately thick sheet, using our method of projection of the dyed fibre images onto the digitiser tablet. The degree of anisotropy is such that all orientation effects are noticeable and scatter of data points is moderate, yet the sheet is not so highly orientated as to be atypical of what one might encounter in industrial production.

Figures 9 through 12 show the experimental data points for the fibre orientation plotted in Cartesian coordinates (frequency of occurrence versus angle of orientation in  $5^\circ$  increments). There are also curves plotted for the single cosine term, and elliptical functions, all under the assumption that  $\mu_0 = 0$  (symmetry edge or an axis of a test specimen), whereas the curves of the von Mises function were plotted without this assumption; the result of this is that the von Mises curves are displaced by approximately 0.1 radian in figures 9, 10 and 11. If the  $\mu_0$  parameter is incorporated in the other functions, they too are displaced, demonstrating that the edges of the sheets were not perfectly aligned with the natural symmetry of the paper.

Determination of the actual axes of preferred orientation by use of the mean direction parameter  $\mu_0$  not only enables better

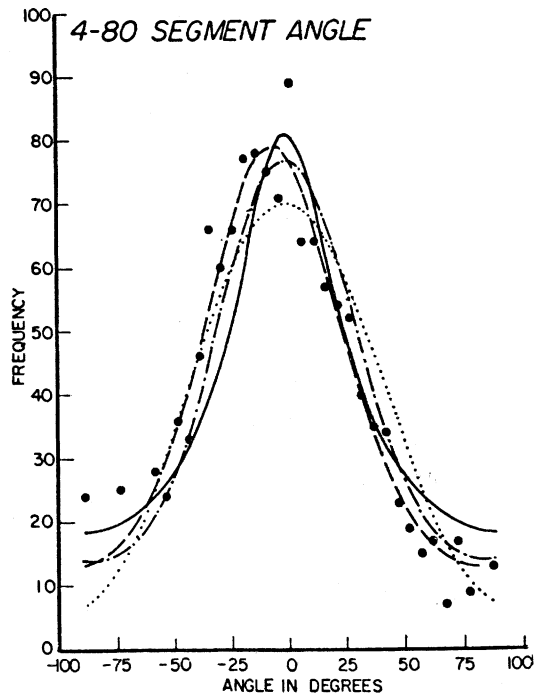


Fig 10—Frequency data for fibre segment angular orientations. Legend: cf. Figure 9.

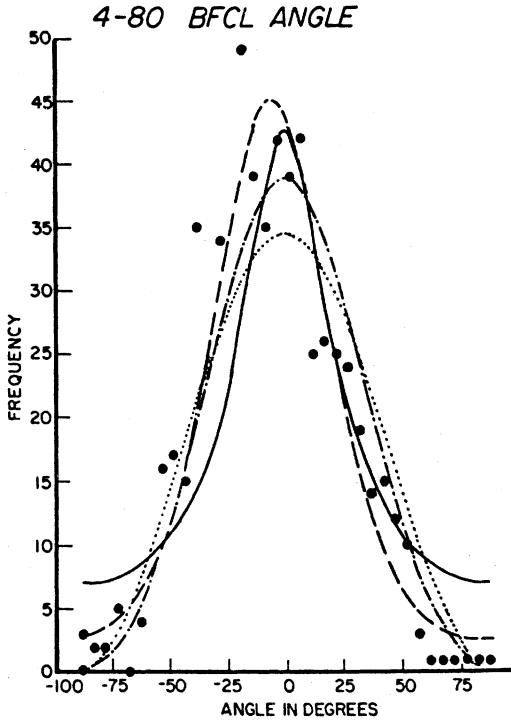


Fig 11—Frequency data for the angular orientations based on best fit to segment midpoints. Legend: cf. Figure 9.

modelling and testing of mechanical behaviour, it also improves the goodness of fit of the distribution function curves. The values for probability presented in Table 2 all have been calculated on the basis of adjusting for the actual mean direction. If one compares these data with those of unadjusted curves (assumption that  $\mu_0 = 0$ ), a substantial difference is often found. For example, the goodness of fit of the elliptical function to the end-to-end data points of specimen 4-80 is 31.1 percent in Table 2, a very satisfactory probability; when the same  $\zeta$  value (i.e. same shape of ellipse) is employed under the assumption

that the data are symmetrical ( $\mu_0 = 0$ ), the probability drops to 1.1 percent. Figure 12 presents the cumulative distribution data for end-to-end orientation.

Figures 13 and 14 show the data points for end-to-end length distribution and cumulative distribution. An Erlang distribution function is used to curve-fit these data. Results for length distribution are tabulated in Table 3.

### Discussion of results

#### Characteristics of the orientation distribution functions. Goodness of fit.

Examination of Table 2 and figures 9 to 12, show that certain characteristics in the angular distribution functions lead to the conclusion that, while some functions are usually superior for describing fibre orientation data, there is no one function that is inherently superior under all conditions. This point cannot be too much emphasised, since every fibre network is different. The results we present here are from one very limited example incorporating only one level of anisotropy.

As previously noted, the incorporation of a mean direction parameter

tests, among other things, the hypothesis that the set of data points is symmetrical. In figures 9 to 11, the only function to be plotted with  $\mu_0 \neq 0$ , the von Mises function, demonstrates that there is some statistical displacement of the data from an axis through  $0^\circ$ , and that the axes of symmetry are rotated. In figure 9 the peak of the von Mises curve is displaced by  $-7.1^\circ$ , in figure 10 by  $-5.7^\circ$ , and in figure 11 by  $-6.1^\circ$ .

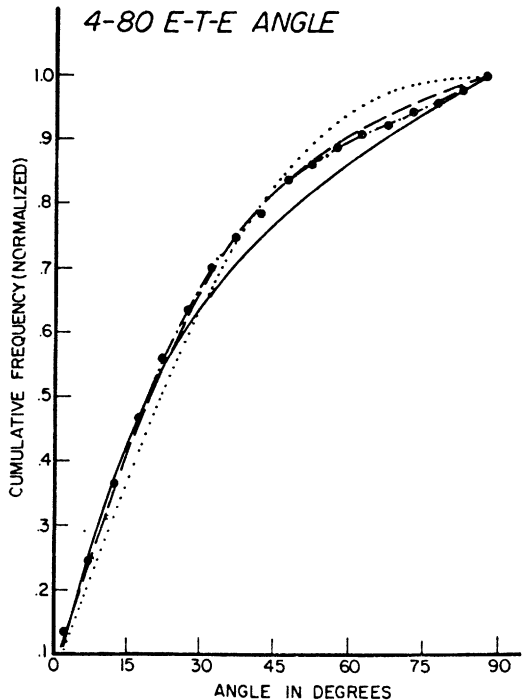


Fig 12—Cumulative frequency data for fibre end-to-end angular orientations. Legend: cf. Figure 9.

Shape Factors: K	Von Mises		Elliptical	Single Cosine Term	Two Cosine Term	
	$\mu_0$			$a_1$	$a_1$	$a_1$
End-to-end angle	1.12	-0.12	2.43	0.97	0.97	0.31
Segment angle	0.91	-0.10	2.10	0.83	0.83	0.18
BFCL angle	1.41	-0.11	2.45	1.00	1.15	0.18

P by  $\chi^2$  test  
for frequency  
%

End-to-end angle	64.2	31.1	0	60.5
Segment angle	45.6	2.3	$8.4 \times 10^{-6}$	48.3
BFCL angle	1.4	$8.5 \times 10^{-9}$	1.5	27.2

P by  $\chi^2$  test  
for cumulative  
frequency, %

End-to-end angle	99.9+	44.2	4.0	99.9+
Segment angle	99.9+	3.0	25.2	99.9+
BFCL angle	66.0	$2.1 \times 10^{-9}$	2.6	99.9+

Table 2

Shape factors, goodness of fit\* of function to data, and goodness of fit\* to cumulative data by Chi-squared test for 4 orientation distribution functions with results from specimens of the 4-80 pulp.

\* First fit - subject to improvement by further adjustment of parameters, and additional Chi-squared testing

Each type of function has certain peculiarities. The single cosine term curve in figure 9 has a peak substantially lower than the others, indicative of its inability to represent highly orientated sheets with high accuracy.

The two-cosine term curve in figure 9 shows local minima at  $65^\circ$ : when the material has an extremely high degree of orientation, these minima may actually lie below the x-axis, thus generating a theoretical distribution that has no physical validity for part of the curve, even though the shape parameters  $a_1$  and  $a_2$  give an acceptable match to the data on other parts of the curve. The elliptical function generally shows a poor fit to the data at fibre orientation angles greater than  $50^\circ$  from the axis of symmetry (see also figures 10 and 11).

We note from the limited base of data that we have generated that the highest probabilities for the fit of the cosine functions tend to occur for the relatively unorientated papers, the highest von Mises probabilities lie in the middle range of orientation, and the best elliptical fits occur when data for very highly orientated material are matched to that function.

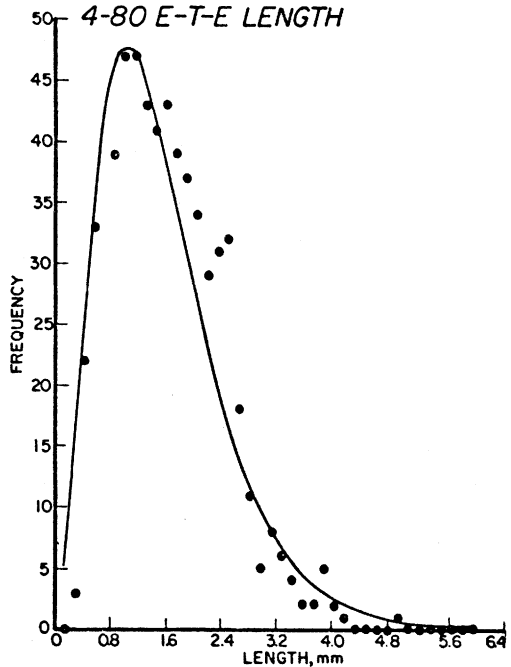


Fig 13—Frequency data for fibre end-to-end length measurements in 0.2 mm increments compared with an Erlang distribution.

	End-to-end Length	Segment Length	Total Length
Shape parameter c	3	4	4
Scale parameter b	0.527	0.191	0.414
P by Chi-squared test for frequency %	7.3	0	0.87
P by Chi-squared test for cumulative frequency, %	79.4	0.01	94.7

Table 3

Shape and scale factors for Erlang probability density function, goodness of fit of function to data by Chi-squared test, and goodness of fit to cumulative data, for 4-80 pulp results.

Overall, the percent probability P that the distribution function describes our data is highest for the two cosine term, closely followed by the von Mises function (see Table 2). Somewhat less accurate is the elliptical function. The single cosine term function is seen generally to be the least accurate. However, there are several exceptions to this ranking, even in our limited data: we believe that all of these functions have utility and that one can use different functions for different levels of anisotropy and other variability with profit.

#### Characteristics of the cumulative distributions

In figure 12 and Table 2 further confirmation is seen that the von Mises and two cosine term functions describe the data for 4-80 specimens with greater precision than do the elliptical and single cosine term. The accuracy of the latter is exceeded by the elliptical function in describing the cumulative frequencies of orientations based on lines connecting the ends of the fibres, but the elliptical fit is poor for segment angular orientations

and very poor for the best fit of segment centre-line points. For two of the three measurement techniques used, the probability exceeds 99.9% that the cumulative frequency is represented by the von Mises function; this probability level is achieved in all three cases by the two cosine term function (see Table 2).

Observations concerning the length distributions

4-80 E-T-E LENGTH

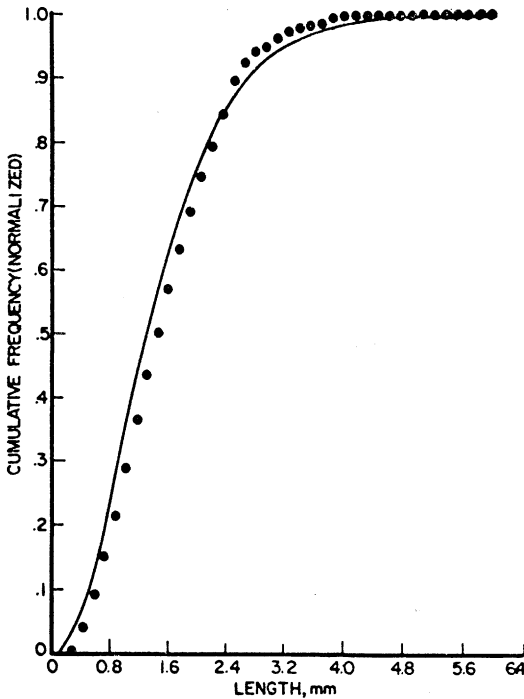


Fig 14—Cumulative frequency data for fibre end-to-end length measurements compared with cumulative Erlang distribution.

As one can see from figures 13 and 14 and Table 3, an Erlang function fits the observed length distributions in an acceptable way, except for the case of fibre segment lengths; perhaps a larger segment length data base is needed. It has been observed<sup>(2,18)</sup> that the length distribution makes a significant contribution to elastic properties in the case of low-density paper but not for high density sheets<sup>(17)</sup>.

On the basis of a very limited amount of data, it appears possible that there is some periodicity or preferred orientation of fibres according to length distribution. If so, the result may have significant structural implications<sup>(34)</sup>.

However, we do not yet have sufficient results to draw any conclusions.

Relations between orientation functions:  
comparison and application of results

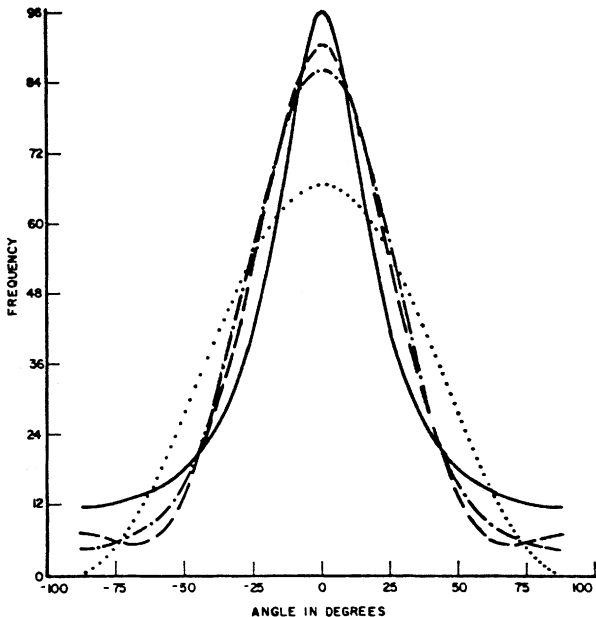


Fig 15—Elliptical (solid line), single cosine term (dotted line) and two cosine term (dot-dashed line) distributions adjusted for best fit to a von Mises distribution (dashed line) with shape parameter  $K = 1.5$ .

In figure 15, a graphical comparison is shown of the four distributions that illustrate some of the mathematical inter-relationships between the functions. In this figure, a plot is made of a von Mises distribution for  $\mu_0 = 0$  and arbitrarily assigned  $K = 1.5$  (corresponding to the highest anisotropy observed in series 5 sheets). An attempt is then made to adjust

the other 3 functions to fit the von Mises curve using the least square method. It is seen that no congruence occurs: the best-fitting elliptical function generates a curve between  $-50^\circ$  and  $50^\circ$  that is narrower and higher, while the cosine function curves are wider and lower. In the  $50^\circ-90^\circ$  range, other disparities occur. We include this illustration to emphasise that the choice of distribution function may be different for each data set: there is no 'right' function, nor a universal correspondence between data and function or function and function.

The four fibre orientation distributions can be compared theoretically by selecting one of the distributions as a reference. For this purpose, one can neglect many of the factors that influence paper elasticity and focus attention only on those factors that depend on fibre orientation. Following the development given above and relations (19), we can compare all of the distribution functions by assigning for each distribution the corresponding values for the Fourier coefficients. For the present comparison it suffices to assume the paper is freely dried and therefore only the coefficients  $a_1$  and  $a_2$  are required. The coefficients  $a_1$ ,  $a_2$  are given for the elliptical and Von Mises distributions by relations (27) and (28). The coefficients for the single cosine, two cosine, and elliptical distributions were selected by least squares analysis to match the von Mises distribution for each choice of the shape parameter  $K$ .

Since it is of interest to investigate the influence of the choice of distribution function on the predicted elastic properties, the quantities

$$E_{xy}^{**} = (8E_x^* \rho_x^a) / (\omega_{s\ l\ s\ f\ o} \varphi_{E^*}^a), \quad E_{yx}^{**} = (8E_y^* \rho_y^a) / (\omega_{s\ l\ s\ f\ o} \varphi_{E^*}^a)$$

and

$$G_{xy}^{**} = (8G_{xy}^* \rho_{xy}^a) / (\omega_{s\ l\ s\ f\ o} \varphi_{E^*}^a)$$

and  $v_{xy}$ ,  $v_{yx}$  are plotted in figures 16 to 20. The von Mises distribution was taken as the reference. The von Mises parameter

K was assigned values of 0.1, 0.3, 0.5, 0.7, 0.9, 1.1, 1.5, and 2.0. Corresponding values of the elastic parameters were calculated and plotted with the prediction from the von Mises distribution as the abscissa.

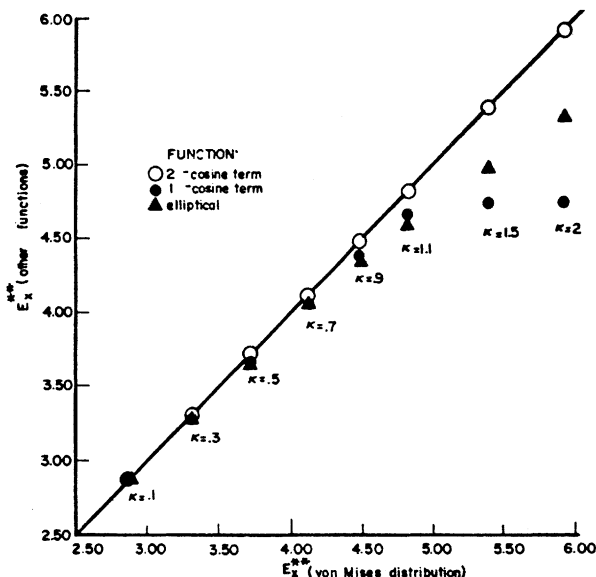


Fig 16—Influence of choice of distribution function on two-dimensional anisotropic elastic constants of paper.

1. Prediction of  $E_x^{**}$  (MD modulus of elasticity) for von Mises = two cosine term distributions (solid line) vs. elliptical (black triangles) and single cosine term (black circles) distributions corresponding to 8 values of the shape parameter  $\kappa$ .

In this theoretical comparison, there is no discernible difference between the two cosine term and the von Mises distributions. The least squares procedure picks essentially the same values for  $a_1$  and  $a_2$  as those corresponding to the Fourier expansion of the von Mises distribution. Inspection of figures 16

to 20 shows that the single cosine term distribution predicts a constant value of  $G_{xy}^{**}$  as the degree of orientation changes. This is because the constant  $a_2 = 0$  for the single cosine term distribution and  $G_{xy}^{**} = 1 - a_2/2$ .

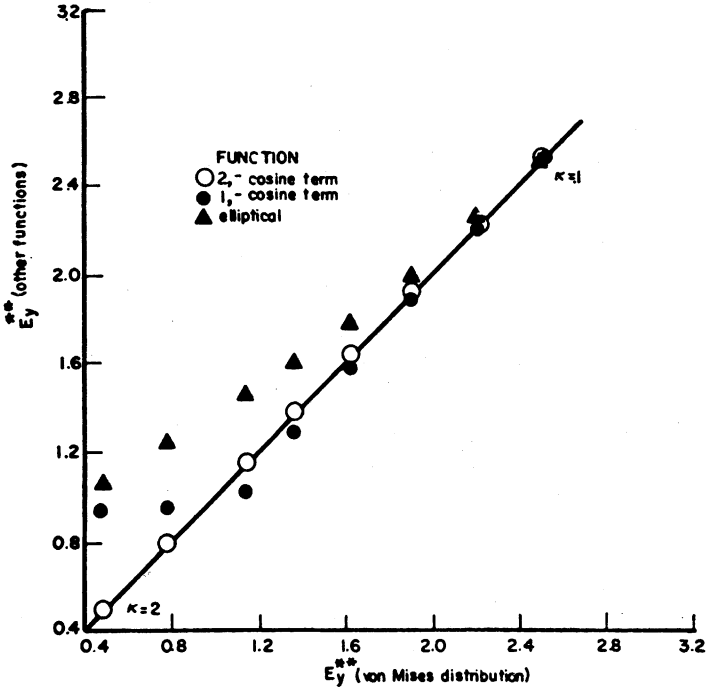


Fig 17—Influence of choice of distribution function on two-dimensional anisotropic elastic constants of paper.  
 2. Prediction of  $E_y^{**}$  (CD modulus of elasticity) for von Mises = two cosine term distributions (solid line) vs. elliptical (black triangles) and single cosine term (black circles) distributions corresponding to 8 values of the shape parameter  $\kappa$ .

The figures show that  $E_x^{**}$ ,  $E_y^{**}$ ,  $\nu_{xy}$  and  $\nu_{yx}$  are well approximated by the single cosine term distributions when the value of  $K < 1.0$ .

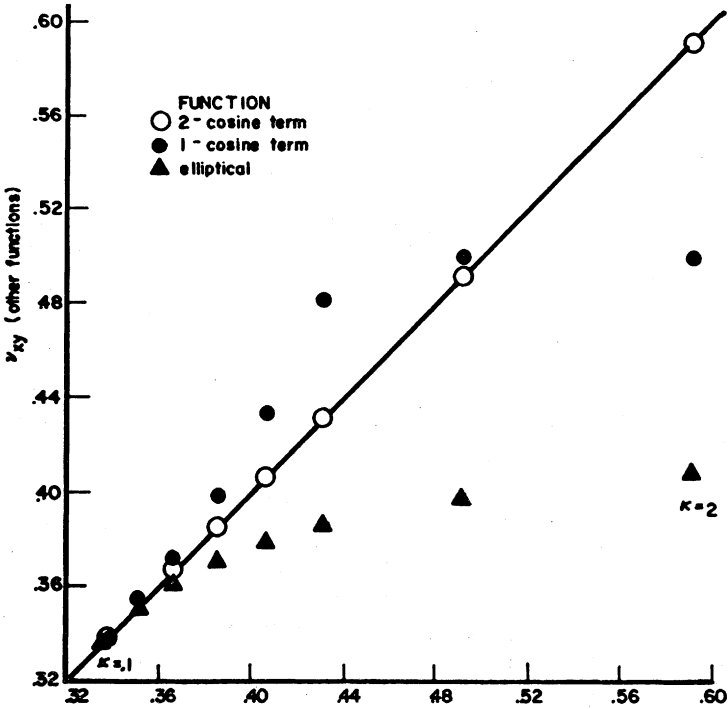


Fig 18—Influence of choice of distribution function on two-dimensional anisotropic elastic constants of paper.

3. Prediction of Poisson ratio  $\nu_{xy}$  for von Mises = two cosine term distributions (solid line) vs. elliptical (black triangles) and single cosine term (black circles) distributions corresponding to 8 values of the shape parameter  $\kappa$ .

The elliptical distribution provides a better approximation of  $G_{xy}^{**}$  and  $E_x^{**}$  than the single cosine term distribution but appears to provide a less accurate prediction of  $E_y^{**}$ ,  $\nu_{xy}$ , and  $\nu_{yx}$ .

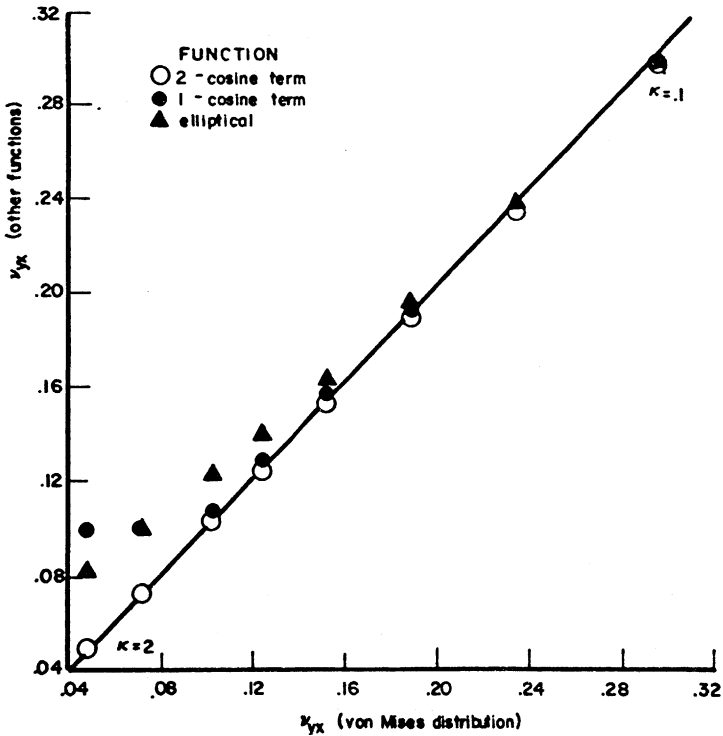


Fig 19—Influence of choice of distribution function on two-dimensional anisotropic elastic constants of paper.

4. Prediction of Poisson ratio  $\nu_{yx}$  for von Mises = two cosine term distributions (solid line) vs. elliptical (black triangles) and single cosine term (black circles) distributions corresponding to 8 values of the shape parameter  $\kappa$ .

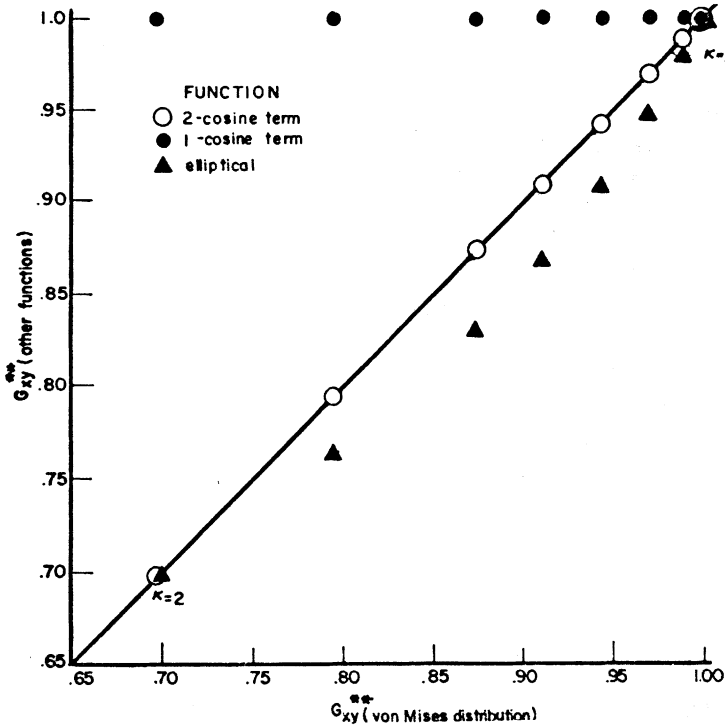


Fig 20—Influence of choice of distribution function on two-dimensional anisotropic elastic constants of paper.

5. Prediction of in-plane shear modulus of rigidity  $G_{xy}^{**}$  for von Mises = two cosine term distributions (solid line) vs. elliptical (black triangles) and single cosine term (black circles) distributions corresponding to 8 values of the shape parameter  $\kappa$ .

Evaluation of drying restraint stiffening parameter H.

As shown in relations (19), the drying restraint conditions can be expected to influence the paper anisotropy. Although the simple form of relation (15) may not perfectly describe the stiffening phenomenon, the use of (15) permits one to investigate

the expected influence of different drying restraint conditions on the elastic properties through (19), providing the value of the drying restraint stiffening parameter  $H$  can be estimated and the sheet shrinkage strains  $a_x M$  and  $a_y M$  are known. The stiffening parameter  $H$  can be estimated from the experimental results of Setterholm and Chilson<sup>(19)</sup>. In their work, the samples were handsheets, and hence were characterised by an isotropic fibre orientation distribution and restrained uniaxially. The expression for  $E_x^* = E_y^* = E$  from ref<sup>(19)</sup> was used with  $a_1 = a_2 = a_3 = 0$ . The drying shrinkage for Setterholm and Chilson's experiments was estimated to be 6%. Based on these assumptions, the value of  $H$  corresponding to their experiments was found to lie in the range 10 to 30. The calculated value of  $H$  was found to depend on the choice of restraint conditions. This finding suggests that  $E_f^a$  may depend on  $e_{ND}$  raised to some power. This behaviour can be readily incorporated into the theory described above; however, it is suggested that more experimental work is needed before the choice of the most satisfactory form for the stiffening relation can be made.

Comparison of mechanical tests and theoretical predictions regarding orientation anisotropy

A series of tests was carried out with the intent of testing the capability of relations (19) to predict the influence of fibre orientation distribution. As mentioned above, 5 series of papers were prepared at the Swedish Forest Products Research Laboratory using a 'Formette Dynamique' apparatus. The samples were dried by placing them on a metal plate. Thus, the samples that were made were very flat after drying. The exact conditions of restraint are not known for this experimental procedure. One might expect that the procedure would correspond to completely uniform restraint, i.e.,  $e_{xD} = e_{yD} = 0$ . This condition would be expected to result in different stiffening effects for different orientation directions in as much as the shrinkage strain  $a_x M$  and  $a_y M$  must depend on fibre orientation distribution (cf. Gallyay<sup>(20)</sup>)

and de Ruvo<sup>(21)</sup>). In fact, if the x-direction corresponds to the 'machine direction' one would expect the fibres that are aligned in the y-direction to experience more stiffening since  $a_y M > a_x M$ . This will be expected to reduce the observed anisotropy of the Young's moduli from that anticipated on the basis of fibre orientation effects. Based on the estimate of the stiffening parameter H from Setterholm and Chilson's<sup>(19)</sup> experiments that was discussed above, the magnitude of the elastic modulus anisotropy due to drying restraint can be estimated by direct application of relations (19). In making these calculations we set  $H = 10$  and  $(a_x M + a_y M)/2 = 0.06$ . Young's modulus measurements of  $E_x^*$  and  $E_y^*$  were made for each orientation level from 1 to 5. Using the procedures that were discussed in detail above, estimates were made of the orientation parameters  $a_1$ ,  $a_2$  and  $a_3$ , the elliptical distribution parameter  $\zeta$ , and the von Mises parameter K. A comparison between the theoretical and experimentally obtained ratios  $E_x^*/E_y^*$  was made by plotting the ratio predicted from relations (19),  $(E_x^*/E_x^*)_{pre}$ , versus the ratio obtained from mechanical testing,  $(E_x^*/E_y^*)_{exp}$ . Interestingly, it was found that relations (19) closely predict the experimentally observed results when the sheet was assumed to have been dried under conditions of no restraint. Evidently the procedure of drying the samples on a metal plate was not characterised by uniform restraint. In fact, this procedure is apparently closer to freely dried conditions in so far as loading the fibres during the drying process is concerned.

The results of the experimental-theoretical comparison are illustrated in figure 21. The experimental scatter present is attributed primarily to the problems associated with conducting the mechanical measurements of Young's modulus, and forming the ratios of values for different samples. Probably a larger number of replications would reduce the amount of scatter. Nonetheless, the results show a remarkably good correlation between the theoretical and experimental values. If there is any tendency for a consistent departure from perfect correlation, it is for the experimental ratios to be higher than the ratios predicted from the observed fibre orientation distributions.

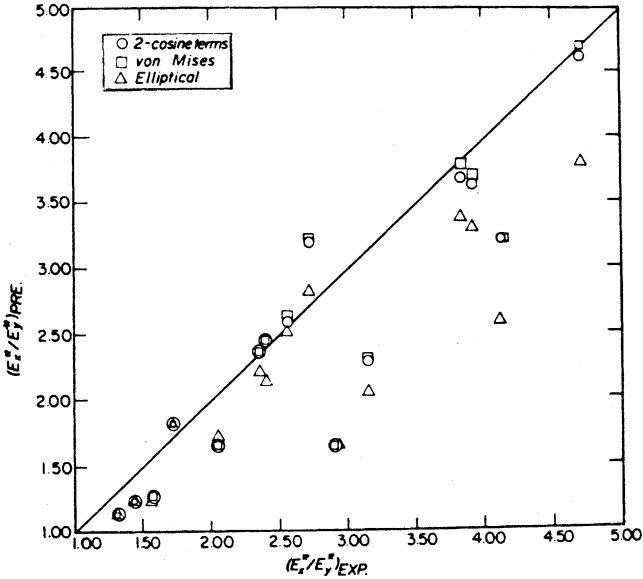


Fig 21—Relation between ratio  $(E_x^*/E_y^*)_{PRE}$  found from relations (19) with direct measurement of fibre orientation and  $(E_x^*/E_y^*)_{EXP}$  found from mechanical tests.

Thus, the mechanical tests showed a higher anisotropy than would be expected on the basis of fibre orientation effect. Any influence of drying restraint would have produced exactly the opposite trend; therefore, the restraint during drying, although perhaps not perfectly predicted by relation (15), was not a factor in this study. As an example, consider the experimental results from the level 5 orientation and  $80\text{g}/\text{m}^2$  basis weight sheets. Based on the estimated value of  $H = 10$  and average shrinkage strain of 6%, the Young's modulus ratio would be predicted to be approximately 3.3. As shown in figure 21, the ratio obtained from the mechanical tests was about 4.5.

It is also of interest to note from figure 21 that the elliptical distribution gives rise to a lower estimate for the  $E_x^*/E_y^*$  ratio at the higher orientation levels than does the von Mises distribution. This behaviour is consistent with that shown in figures 16 to 20 to be characteristic of the elliptical distribution.

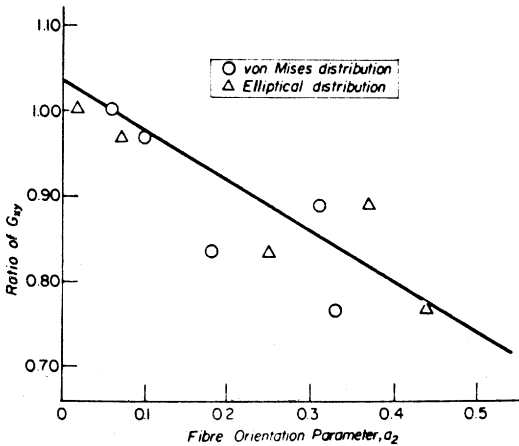


Fig 22—Experimental values of  $G_{xy}^*$  normalized with respect to 1-80 material vs. fibre orientation parameter  $a_2$  (cf. relation (19)).

It was noted above that relations (19) predict that  $G_{xy}^*$  is expected to decrease with increased orientation anisotropy provided that the coefficient  $a_2$  is not dropped. The results for the Young's modulus ratios indicate that drying restraint effects were negligible for the present experimental material. Therefore, relation (19) predicts that  $G_{xy}^*$  is proportional to the quantity  $2 - a_2$ . The experimental values of  $G_{xy}$  were obtained by a torsion pendulum method for the 80g/m<sup>2</sup> basis weight material and the 5 orientation levels. A comparison between the

theoretical and experimental results is shown in figure 22, where the data has been normalised with respect to the level 1 material. Both the predicted and the experimental results are observed to decrease with increasing anisotropy as expected.

It is worth noting that relation (19) can be used as a basis for predicting the elastic constants  $G_{xy}^*$ , and  $\nu_{xy}$ ,  $\nu_{yx}$  from measurements of the Young's moduli in the machine and cross-

machine directions. If the conditions of drying restraint are known or can be reasonably approximated, and if experimental values for  $E_x^*$  and  $E_y^*$  are available, relation (19) can be used to calculate the ratio  $E_x^*/E_y^*$ . It is recommended that the parameters  $a_1$ ,  $a_2$  and  $a_3$  be represented in terms of the von Mises shape parameter  $K$  with the help of eq. (27). Then, the experimentally obtained value of  $E_x^*/E_y^*$  can be used to calculate  $K$ . This value of  $K$  can be used with the remaining relations to estimate  $G_{xy}^*$ ,  $\nu_{xy}$  and  $\nu_{yx}$ . This procedure has been found to give quite satisfactory predictions when employed on the experimental results reported by Jones<sup>(12)</sup>.

#### Theoretical predictions involving length distribution and the coupling parameters a

Inspection of relations (5) through (19) shows that the in-plane elastic properties of a paper sheet depend on basis weight  $\omega_s$ , apparent fibre density  $\rho_f^a$ , apparent fibre modulus  $E_f^a$ , and the length distribution factor  $\phi_{1s}$ .  $E_f^a$  depends not only on the true elastic modulus of the cell wall material but on the degree of bonding of fibres, i.e., the relative bonded area (RBA) and the stiffness of the fibre-to-fibre bonds. Moreover,  $E_f^a$  depends on the loading of the fibre during the drying of the sheet.

The length distribution factor  $\phi_{1s}$  depends, of course, on the actual length distribution of the fibre segments  $l_s$  and, as discussed above, the Erlang distribution with parameters  $b$  and  $c$ , appears to be satisfactory for describing the distributions in paper. The length factor  $\phi_{1s}$  also depends very strongly on the degree of coupling of the fibres to the remainder of the network as described by the coupling parameter  $a$  (cf. relation (7)). The degree of coupling depends both on the bending and shearing of crossing fibres and on the shear stiffness of the fibre-to-fibre bond. Bending and shearing effects predominate when the relative bonded areas are very low as in the case of tissue papers. In the case of moderate density papers, the bending and shearing effects are negligible and the shear stiffness of the fibre-to-

fibre bonds dominates the behaviour of the system. For either coupling mechanism, the effects of length distribution will be important only when the coupling is quite weak. An indication of the magnitude of the length effect can be seen in an example based on the data that has been collected in the present study.

If one confines attention to the moderate density range, the coupling can be approximately expressed in the form

$$aL \doteq 20 \text{ RBA} \frac{L}{w_f} \sqrt{\frac{10G_b}{E_f^a}} \quad (30)$$

The coupling efficiency  $\eta_L$  can be approximated as

$$\eta_L \doteq 1 - 1/2aL \quad (31)$$

Using relation (14), one finds that

$$\varphi_{1s} \doteq 1 - \frac{c}{(c-1)} \frac{w_f}{\langle l_s \rangle} \frac{1}{20 \text{ RBA}} \sqrt{\frac{E_f^a}{10G_b}} \quad (32)$$

The parameter  $c$ , the shape parameter for the Erlang distribution, was found to have the value 4 for the case of the  $80\text{g/m}^2$  basis weight level 4 orientation sample material. For this material, it was estimated that  $\text{RBA} = 0.5$ , the average segment length  $\langle l_s \rangle$  was found to be 0.76 mm, and the ratio  $w_f/\langle l_s \rangle$  was taken to be  $1/40$ . Of course, the value of  $\varphi_{1s}$  now depends on knowing the bond shear stiffness  $G_b$ . Unfortunately, there is no experimental data presently available that can be used to estimate  $G_b$ , however some indications of the dependence of  $\varphi_{1s}$  on  $G_b$  can be obtained from relation (32). For example, if the value of  $G_b/E_f^a$  is taken as 10,  $\varphi_{1s}$  is found to be 0.96. If the bond stiffness were decreased to make the ratio  $10^{-4}$ , then  $\varphi_{1s}$  would be found to have the value 0.89. Evidently quite small values of the ratio  $G_b/E_f^a$  would be necessary in order for the length distribution to have a noticeable effect on the

elastic behaviour. It is apparent that more experimental work is needed, especially where papers having substantially different measured values of  $c$  and  $\langle l_s \rangle$  are to be compared. Inasmuch as both the length distribution and the coupling are so closely interrelated it will be necessary to have extensive experimental information concerning the relative bonded area as well. It should also be recognised that even though  $\phi_{1s}$  may not significantly influence the elastic properties, the length distribution may in fact have an important effect on the strength properties of the sheet.

### Acknowledgements

The authors wish to express their sincere appreciation to Clay M. Crosby and Amin Eusufzai of ESPRI and Nitin Uplekar of Heat Extractor Corporation for the valuable contributions they made to assist the progress of the work reported here, and to Drs. Holger Hollmark and Hans Andersson of the Swedish Forest Products Research Laboratory (STFI), our esteemed colleagues and collaborators in this co-operative programme.

### REFERENCES

1. Cox, H.L. Brit. J. Appl. Phys., 1952, 3, 72.
2. Perkins, R.W., Proc. of the Conference Paper Science and Technology: The Cutting Edge (Institute of Paper Chemistry, Appleton, 1980), 89.
3. Carroll, C.W., Formation and Structure of Paper, Vol. 1, Ed. F. Bolam (Tech. Sect., Brit. Paper and Board Makers' Assn., London, 1962), 243.
4. Corte, H. and Kallmes, O.J., Formation and Structure of Paper, Vol 1, Ed. F. Bolam (Tech. Sect., Brit. Paper and Board Makers' Assn., London, 1962), 13.
5. Forgacs, O.L. and Strelis, I., Pulp Paper Mag. Canada, 1963, 64(1), T-3.

6. Mardia, K.V., *Statistics and Directional Data*, (Academic Press, New York, 1972).
7. Judt, M., *Das Papier*, 1958, **12**(21/22), 568.
8. Glynn, P., Jones, H.W.H. and Gallay, W., *Pulp Paper Mag. Canada*, 1959, **60**(10), T-316.
9. Ranger, A.E. and Hopkins, L.F., *Formation and Structure of Paper*, Vol. 1, Ed. F. Bolam (Tech. Sect., Brit. Paper and Board Maker's Assn, London, 1962), 311.
10. Prusas, Z.C., *Tappi*, 1963, **46**(5), 325.
11. Kallmes, O.J. and Bernier, G., *Tappi*, 1964, **47**(11), 649.
12. Jones, A.R., Ph.D. Thesis, Institute of Paper Chemistry, Appleton, 1967. Univ. Microfilms, Ann Arbor, 1972.
13. Setterholm, V.C. and Kuenzi, E.W., *Tappi*, 1970 **53**(10), 1915.
14. Yang, C.F., Ph.D. Thesis, Univ. Washington, Seattle, 1975.
15. Danielsen, R. and Steenberg, B., *Svensk Papperstidn.*, 1947, **50**(13), 301.
16. Hastings, N.A., and Peacock, J.B., *Statistical Distributions*, John Wiley & Sons, New York, 1975, 54.
17. Chang, J.S., M.S. Thesis, Syracuse Univ. (in preparation), 1981.
18. Hollmark, H., Andersson, H. and Perkins, R.W., *Tappi*, 1978, **61**(9), 69.
19. Setterholm, V.C. and Chilson, W.A., *Tappi*, 1965, **48**(11), 634.
20. Gallay, W., *Tappi*, 1973, **56**(11), 54.
21. de Ruvo, A., Lundberg, R., Martin-Löf, S. and Söremark, C., *The Fundamental Properties of Paper Related to its Uses*, Vol. 2, Ed. F. Bolam (Tech. Div., Brit. Paper and Board Ind. Fed., London, 1976), 785.

## Transcription of Discussion

**Discussion following papers given by Prof. R.W. Perkins,  
and by Dr. C. Fellers.**

Prof. J. Silvy, Ecole Francaise de Papeterie

Firstly, in the example given of the length distribution, was the sample beaten?

Secondly, how long does it take to obtain the information from a complete run in your process?

Prof. R.W. Perkins, Syracuse University, USA

I don't think the pulp was beaten, but I am not certain because it comes ready prepared from STFI. I do know that it was a bleached softwood kraft.

Our procedure is quite rapid, because although the digitising must be done manually, to do it the cursor need only be placed on each individual point. No intermediate stopping or steps are necessary. The total time for a run involves the manufacture and digitising, and this was done for all 600 fibres per sample.

Prof. J. Silvy

As a point of information, it takes us an hour and a half to digitise 1800 fibres at Grenoble.